IEEE Access
Multidisciplinary | Rapid Review | Open Access Journal

Received 3 May 2024, accepted 16 May 2024, date of publication 22 May 2024, date of current version 4 June 2024.

Digital Object Identifier 10.1109/ACCESS.2024.3404123

RESEARCH ARTICLE

Assessment of SMOS Root Zone Soil Moisture: A Comparative Study Using SMAP, ERA5, and GLDAS

NITU OJHA, ALI MAHMOODI, ARNAUD MIALON, PHILIPPE RICHAUME, SYLVAIN FERRANT, AND YANN H. KERR, (Life Fellow, IEEE)

Centre d'Étude Spatiale de la BIOsphère (CESBIO-UPS-CNRS-IRD-CNES-INRAE), 31401 Toulouse, France

Corresponding author: Nitu Ojha (nitu-kumari.ojha@univ-tlse3.fr)

This work was supported in part by the Center National d'Études Spatiale (CNES), Terre Solide, Océan, Surfaces Continentales et Atmosphère (TOSCA); and in part by the Center Aval de Traitement des Données SMOS (CATDS) Program.

ABSTRACT Root zone soil moisture (RZSM) refers to the amount of water present in the soil layer where plants can freely absorb water, and its information is crucial for various applications such as hydrology and agriculture. SMOS and SMAP remote sensing satellites provide soil moisture (SM) data on a global scale but limit their sensing capability to a depth of approximately 5 cm. However, for a comprehensive understanding of soil water content in the root zone, a deeper insight into RZSM is essential, which extends from 5 cm to 100 cm. Hence, to bridge the gap between the surface SM and RZSM, SMOS surface SM information (5 cm) was integrated into the root zone (100 cm) using a simple subsurface physical model. SMOS RZSM data are available on a global scale with 25 km sampling on EASE grid 2, which provides a daily temporal scale from 2010 to the present. The main aims of this study were to i) check the efficacy of a simple model-based approach and ii) investigate the importance of remote sensing SM observations for the retrieval of RZSM. Here, we investigate the benefit of the simple model-based approach by comparing SMOS RZSM (simple model) and SMAP, ERA5, and GLDAS RZSM (complex model or data-assimilation) with in-situ SM. We then investigated the role of remote sensing SM observation in the retrieval of RZSM by comparing SMOS RZSM and SMAP RZSM products over rice-irrigated areas for dry seasons (minimal rainfall) in Telangana, South India. First, SMOS RZSM was evaluated with in-situ SM data for four distinct networks: SCAN, HOBE, SMOSMANIA, and Amma catch from 2011 to 2017. The results between SMOS RZSM and in-situ SM show an average correlation coefficient between 0.54 and 0.8 with an average unbiased root mean square difference (ubRMSD) within the threshold of 0.04 m^3/m^3. The average correlation coefficient between the RZSM and in-situ SM for the SMOS and SMAP RZSM shows better performance in the range (0.55 to 0.93) than the ERA5 and GLDAS RZSM in the range (0.20 to 0.93). Finally, the outcomes of SMOS and SMAP RZSM over irrigated areas show that only SMOS RZSM captures changes in SM dynamics due to irrigation, particularly during the dry season.

INDEX TERMS Surface soil moisture, root zone soil moisture, SMOS, SMAP, GLDAS, ERA5.

I. INTRODUCTION

SM is a crucial element of the land surface and atmosphere [1]. Hence, SM is useful for various applications, such as hydrology [2], agriculture [3], climatology [4], and meteorology [5]. SM is highly variable in space and time, and remote sensing has been found to be an effective method for capturing this variability on a global scale [6]. Various sensors, such as passive, active, and optical/thermal sensors, are used to retrieve SM data on regional or global scale.

L-band radiometers such as Soil Moisture and Ocean Salinity (SMOS) [7] and Soil Moisture Active Passive (SMAP) provide global SM at a sensing depth of 5 cm [8], but there is a significant challenge in obtaining SM information

The associate editor coordinating the review of this manuscript and approving it for publication was Gerardo Di Martino.

at depths that are relevant to the root zone of plants. SM information at the root zone is useful for various applications such as hydrological modeling [9], land surface modeling [10], weather forecasting [11], agricultural productivity [12], and flood /drought monitoring [13]. Despite advancements in remote sensing, direct observation of RZSM using satellites remains a challenge.

Various methods exist for measuring RZSM, including ground measurements [14], data-driven [15], data assimilation [16], [17], [18], satellite observations [19], [20]. Ground measurements provide direct measurements like time-domain reflectometry (TDR) [21] or cosmic-ray neutron probe [22], but limit its applicability in spatial coverage. Data-driven approaches such as time series analysis and machine learning show promise but require high-quality input data for training a model [23], [24]. Data-assimilation methods, like Global Land Data Assimilation (GLDAS) [25], the fifth-generation European Centre for Medium-Range Weather Forecasts atmospheric analysis product (ERA5) [26], Soil Moisture Active Passive (SMAP) level-4 RZSM product [27], combines satellite observations and numerical models and provides more accurate results but are computationally intensive. Satellite observations, for eg., ERS scatterometer [19], [28], and SMOS [20], utilize surface SM to estimate RZSM, by considering a link between surface SM and RZSM [29], [30].

Wagner et al. [19] proposed a simple water model to estimate RZSM from satellite observations. The model integrates surface SM information (satellite observations) into the RZSM based on hydraulic conductivity, which depends on the time required to transfer water from the surface to the deeper soil layer. The SMOS RZSM is estimated using a similar model but modified using recursive exponential filters [31], similar to Albergel et al. [32], including soil texture information, as discussed by Al Bitar et al. [33]. The SMOS RZSM has been available from 2010 to the present on a global scale. Several studies have validated the SMOS RZSM but are limited to specific regions [34]. A recent study showed that SMOS and SMAP surface SM data capture irrigation signals that are not recognized in SMAP RZSM [35]. However, there is a lack of global and comprehensive studies on SMOS RZSM under varying climatic conditions and their relevance in the context of irrigation.

The main objective of this study was to assess the quality and accuracy of the SMOS RZSM with in-situ SM under different climatic conditions and to compare it with other RZSM products (ERA5, SMAP, and GLDAS) to evaluate their capability to account for human-induced changes, particularly irrigation. In this context, the SMOS RZSM was evaluated using ground-based measurements collected from ISMN networks for Amma Catch, HOBE, SCAN, and SMOSMANIA from 2011 to 2017. The SMOS RZSM was compared to other RZSM products (ERA5, SMAP, and GLDAS) in 2017. Finally, the performance of RZSM products was examined in dry- irrigated areas in Telangana, India.

II. MATERIALS AND METHODS

A. IN-SITU MEASUREMENT FOR VALIDATION

In-situ RZSM measurements were selected from the ISMN because they provide SM information at different depths for several networks (Dorigo et al., 2011). Four networks were selected from ISMN from 2011 to 2017: Amma Catch, HOBE, SCAN, and SMOSMANIA. All in-situ measurements selected from the ISMN underwent a quality control procedure performed by the ISMN, and only the highest quality in-situ measurements (described in the ISMN criteria) were used for validation. The idea is to select only four networks from the ISMN, as they show better performance with surface SM [36], [37], [38] and fulfill the quality criteria of RZSM. A brief description of each in-situ network is presented below.

1) AMMA CATCH (LEBEL ET AL [39])

This observatory includes mesosites named Benin, Niger, and Mali/Senegal. Benin has a Sudanian climate, with an average rainfall of 1200 mm/yr, and is located at the southernmost site of the observatory. Niger is situated southwest of Niger and has a Sahelian climate, with an average rainfall of 450-600 mm/yr. Mali/Senegal has a semi-arid climate with an average rainfall of 200-400mm/yr, and is located in the northeast. In Benin, the land is covered by crops; Niger by crops and pastoral land and Mali by pastoral land. The soil texture was sandy clay loam in Benin and sandy loam in Niger.

2) HOBE (BIRCHER ET AL. [40])

The HOBE observatory is situated in the Skjern catchment of Western Denmark. The area has temperate climatic conditions, with an average rainfall of 1050 mm/yr. The land is covered by agriculture. The soil texture was a sandy loam. A Decagon 5TE sensor was used to measure volumetric SM at depths of 0.05 m, 0.25 m, and 0.55 m.

3) SCAN (SCHAEFER ET AL. [41])

The SCAN network is located in the United States, and the system focuses on covering the agricultural areas of the U.S. The region is cold semi-arid in the west, humid continental in the north, and humid temperate in the south, lower midwest, and middle Atlantic states. The annual average rainfall is between 710 mm/yr to 1600 mm/yr. The land was covered by agriculture, shrubs, and pastures. The soil texture is silty loam in the central northeast, northeast, south, and central northwest; sandy loam in the center, northwest, and southwest; clay loam in the southeast; and silt in the west. Hydraprobe sensor used to measure soil moisture at a depth range from 0.2m to 2.3 m.

4) SMOSMANIA (CALVET ET AL. [36])

The SMOSMANIA network is located in southern France. The area has a Mediterranean climate, with average annual rainfall ranging from 500 mm to 1734 mm. The land is covered by croplands and grasslands. It consists of 21 sites. The soil texture is sandy loam, clay loam and loam. A theta

TABLE 1. Description of the in-situ data.

Network	Country	Climate	Land cover	Soil texture	Depth of the sensors	References
Amma Catch	Benin, Niger	Tropical, Arid	Savannas	Sandy clay loam, Sandy loam	5 cm, 10 cm, 20 cm, 40 cm	Lebel et al. [39]
HOBE	Denmark	Temperate	Croplands	Loamy sand	5 cm, 20-25cm, 50-55cm	Bircher et al. [37]
SCAN	United states	Temperate	Grasslands	Silt loam, Silty clay loam, Loamy sand	5 cm, 10 cm, 20 cm, 50 cm	Schaefer et al. [41]
SMOSMANIA	France	Semi-arid	Cropland	Clay loam, Sand loam, Loam	5 cm, 10 cm, 20 cm, 30 cm	Calvet et al. [36]

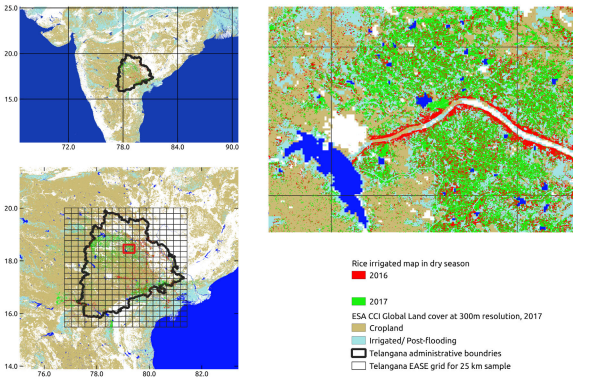

FIGURE 1. Rice irrigated map in dry season for 2016 and 2017 in Telangana, South India.

probe sensor was used to measure the SM at different depths ranging from 5 to 30m.

The different depths of the in-situ networks that contribute to the deepest RZSM are listed in Table 1.

B. IRRIGATED AREA

Figure 1 illustrates the map of the Telangana region and rice irrigation map from 2016 to 2017. As shown in Figure 1, Telangana is highly irrigated area for rice production which is approximately 20 percent, and the extent varies in space (from 3 to 80 percent) and time from one year to another depending on the availability of surface water and groundwater. Flood irrigation has been used for rice cultivation [35], [42]. A rice cover map was produced using Sentinel-2 and ground measurements were performed using a supervised classification algorithm at 10 m [42]. Note that the rice cover map is presented here only for the dry seasons from 2016 to 2019. A rice map for the wet season was not produced because of the limited availability of Sentinel-2 data owing to the cloud cover.

C. SMOS LEVEL-3 SM DATA

The SMOS is a L-band (1.4 GHz) radiometer that covers Earth continuously and globally. It was launched in November 2009. It provides SM on a global scale and a temporal revisit of three days at the equator with an ascending (6 am)/descending (6 pm) overpass on the local solar time. SMOS provides surface SM (0-5 cm) with an expected accuracy of 0.04 m^3/m^3 over particular cases such as low vegetated land with water content less than 5kgm-2 and homogeneous observed scenes [43].

This study used the SMOS CATDS level-3 (CLS1A/D) version 339 daily global SM product for the ascending and descending overpasses. SMOS Level-3 SM products provide SM in the Equal-Area Scalable Earth Grid, Version 2.0 (EASE-Grid 2.0) [44] with a grid sampling of 25 km in netCDF format [45].

D. PRECIPITATION

The Integrated Multi-satellite Retrievals for Global Precipitation Measurement (IMERG) algorithm was developed by the National Aeronautics and Space Administration (NASA). The Global Precipitation Measurement (GPM) satellite mission between NASA and the Japan Aerospace Exploration Agency (JAXA) was launched in 2014. The IMERG algorithm integrates GPM information to provide global precipitation data. Monthly IMERG GPM precipitation data were used to monitor precipitation.

E. NORMALIZED DIFFERENCE VEGETATION INDEX

The Normalized Difference Vegetation Index (NDVI) was calculated from the red and infrared bands of the Moderate Resolution Imaging Spectroradiometer (MODIS). This helps to estimate the growth of vegetation. The monthly NDVI level-3 MOD13A3 version 6, with a spatial resolution of 1 km was gridded using sinusoidal projection.

F. GLDAS RZSM DATA

GLDAS is a high-resolution land surface model that produces optimal land surface states and fluxes by combining satellite and ground observation data using data assimilation techniques [46]. GLDAS was developed by the NASA and the National Oceanic and Atmospheric Administration.

GLDAS version 2.2 uses the NASA Climatology Land Surface Model (CLSM) and other input meteorological parameters from the European Center for Medium-Range Weather Forecasts (ECMWF) and Gravity Recovery and Climate Experiment (GRACE) as satellite observation [25]. It provides a product with a spatial resolution of 0.25°*0.25° at a 3-hour temporal period from February 2003 to the present. The soil moisture depth (2-100) cm was considered as the RZSM layer.

G. ERA5 RZSM DATA

ERA5 is a fifth-generation reanalysis product developed by ECMWF to provide global climate and weather data from January 1979 to the present. ERA5 combines models and observation using 4-Dimensional variational data assimilation to provide a reanalysis product [26].

ERA5 provides data at 0.25°*0.25° spatial resolution for 3-hour temporal period. ERA5 provides SM information for different soil water layers: 0-7 + 7-28 + 28-100 cm. Here, the weighted average of SM at a depth of 7-100 cm is used.

H. SMAP LEVEL-4 RZSM DATA

The SMAP Level-4 RZSM was produced by assimilating SMAP level-1 brightness temperature (Tb) data into the NASA Catchment land surface model [47]. The assimilated SMAP data include the horizontal and vertical polarizations Tb from the ascending and descending half-orbits.

SMAP Level-4 RZSM data are available at 9 km on EASE-Grid 2.0 with a 3-hour temporal period at a global scale. SMAP Level-4 provides SM estimates for the surface (0-5 cm), RZSM (0-100 cm), and profile (0 cm to bedrock depth) layers. SMAP Level-4 RZSM data are available from March 31, 2015, to the present.

I. ESTIMATION OF LEVEL-4 SMOS RZSM

The SMOS Level-4 RZSM was calculated using the SMOS Level-3 surface SM data. The SMOS surface SM undergoes a quality control process, such as Chi-square and Radio Frequency Interference (RFI) probability. The SMOS RZSM was retrieved from the SMOS surface SM using a simple water model [19]. The model was modified by a recursive exponential filter [31], similar to that of Albergel et al. [32], and incorporated soil texture and layer-specific information to retrieve the RZSM globally [33]. The methodology used to calculate SMOS RZSM is described below.

The soil profile was divided into three distinct layers: the uppermost layer, L_0, ranging from 0-5 cm (thickness $d_0 = 5\ cm$); an intermediate layer, L_1, ranging from 5-40 cm (thickness $d_1 = 35\ cm$); and a deep layer, L_2, ranging from 40-100 cm (thickness $d_1 = 60\ cm$).

In the following subscripts, i, is the time index (day) of the time series and the superscript k is the layer index, where $k \in \{0, 1, 2\}$; upper, intermediate, and deep. For a given grid point, the time series of the satellite observed surface SM, SM_i^0, was the uppermost (0-5 cm) surface SM layer. The deeper SM layer from the uppermost surface SM layer for a given time series is computed as follows:

First, for a given time series, the process starts by converting the surface SM SM_i^0 to a soil water index (SWI) SWI_i^0 using scaling Equation (1).

$$SWI_i^0 = log(c * SM_i^0 + a) + b \tag{1}$$

where, the scaling coefficients, a, b are derived from the minimum/maximum surface SM SM_{min}^0 and SM_{max}^0 using (2) and c=1.2 (logarithmic correction).

$$a = SM_{max}^0 \frac{e^{SM_{min}^0} - 1}{1 - e^{SM_{min}^0} - 1} \tag{2}$$

$$b = 1 - log(SM_{max}^0 + a) \tag{3}$$

where SM_{max}^0 (m^3/m^3) and SM_{min}^0 (m^3/m^3) are the SM at saturation and field capacity, respectively, calculated from the pseudo-transfer function using the soil texture information [48].

Subsequently, a sequential filter was employed to calculate the SWI at a given time index, i, and layer index, k > 0, using Equations (4) and (5).

$$SWI_{i+1}^k = SWI_{i=0}^k + Kn_{i+1}^k * (SWI_i^{k-1} - SWI_i^k),\ i \geq 0,\ k > 0 \tag{4}$$

where, $SWI_{i=0}^k$ is initialized to previous SM value, where $k \in \{1, 2\}$

where, Kn_{i+1}^k is computed as:

$$Kn_{i+1}^k = \frac{Kn_i^k}{Kn_i^k + e^{\frac{-DT}{T_k}}},\ i \geq 0 \tag{5}$$

where T_k is the time constant (days) represents the time required to update SM from layer $k-1$ to k. The DT (days) is the time delay interval from the previous update.

According to Darcy's law of conservation of mass in saturated porous media, the time constant is logarithmically related to hydraulic conductivity. Based on this analysis, T_k is computed for a given layer index, $k > 0$ as follows:

$$T_k = \frac{log(K_{sat}) - log(max(K_{sat}))}{log(min(K_{sat})) - log(max(K_{sat}))} * T_{k,int} - T_{k,min} \tag{6}$$

where K_{sat} is the hydraulic conductivity at saturation, $T_{k,int}$ (days) is a constant representing the time interval at k layer and $T_{k,min}$ is the minimum value of T at layer k.

K_{sat} is computed as:

$$K_{sat} = a * (b - c * X_{clay} - d * X_{sand} + e * X_{clay}^2 + f * X_{sand}^2) \tag{7}$$

where, a, b, c, d, e and f are constant calculated from Noilhan and Mahfouf [49] shown below: a = 10-6, $b = 41.5661691$, $c = 5.81989$, d=0.0907123, $e = 5.29268$, $f = 1.20332$.

After calculating the SWI, the absolute SM for a layer k >1 was derived from the SWI through linear scaling between the minimum (SM_{min}^k) and maximum (SM_{max}^k) soil retention capacity of the layer as follows:

$$SM_i^k = (SM_{max}^k - SM_{min}^k) * SWI_i^k + SM_{min}^k \tag{8}$$

A similar step was applied to retrieve the SM values for the intermediate, L_1 and deeper layers, L_2.

Finally, the RZSM (5-100 cm depth) was computed using Equation (9) as the weighted average of the SM values from the two deepest layers, weighted by their respective thicknesses d_1 and d_2:

$$RZSM_i^{5-100} = \frac{d_1 * SM_i^1 + d_2 * SM_i^2}{d1 + d2} \tag{9}$$

The SMOS level-4 RZSM data provides RZSM at 5-100 cm depth with a spatial sampling of 25 km on EASE-Grid 2 at a global scale. It provides RZSM data on a daily temporal scale for both the ascending and descending overpasses. The dataset was freely available on the CATDS platform from 2010 to the present day.

III. RESULTS AND DISCUSSION

The results of this study are discussed in three different sections: first, visual assessment of SMOS RZSM at a global scale; second, evaluation of the SMOS RZSM product with in-situ SM; and third, comparison of SMOS RZSM with other available SMAP, ERA-5, and GLDAS RZSM products.

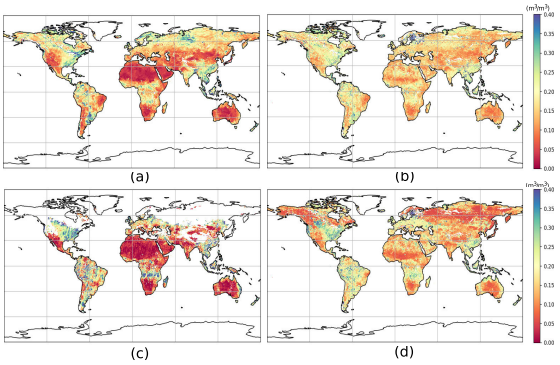

FIGURE 2. Global yearly average map of SMOS surface SM (a) and SMOS-RZSM (b) of 2017 (top) and daily map (3-day average) for SMOS surface SM (c) and SMOS level-4 RZSM (computed from 3 day average surface SM)(d) (below) of April 1, 2017.

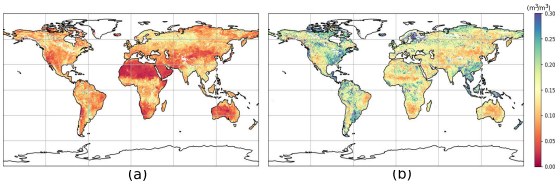

FIGURE 3. Standard deviation of SSM (a) and RZSM (b) for the year 2017.

A. VISUAL ASSESSMENT OF SMOS RZSM AT GLOBAL SCALE

Figure 2 illustrates the annual average and daily maps of SMOS surface SM and RZSM. Low SM values were observed for dry regions, such as the southwestern United States, South Africa, Central Africa, and Southwestern Europe, and higher SM values were observed for wet areas in the northeastern United States, northern Europe, and Southeast Asia but the range of SM values differed in all the maps. More variability was observed in the surface SM in Figure 2(a,c) than in RZSM 2(b,d) for both the annual and daily maps for Eastern Australia and Eastern Arizona, as shown in Figure 3. The variability in surface SM is attributed to climatic factors and anthropogenic activity [50]. On the other hand, RZSM (deeper soil layer) exhibits a gradual response to short-term weather variations. Hence, the SM in the root zone is more stable and preserves long-term memory; this characteristic is not prominent in the surface SM [51].

Figure 4 presents a Hovmoller plot of SMOS RZSM anomalies over Australia from 2010 to 2022 to demonstrate the usefulness of long-term RZSM information for identifying extreme events. The plot illustrates the spatial and temporal variability of the RZSM along latitude. RZSM anomalies were calculated to remove seasonal effects that occured at the regional scale. The SMOS RZSM anomalies shown in the Hovmoller plot are calculated as follows:

$$RZSM_i^{anom} = RZSM_i - \frac{1}{N}\sum_{year} RZSM_{i,year} \qquad (10)$$

where, i (days) $\in \{1 \ldots 365\}$. For the currently available dataset, $year \in \{2010 \ldots 2022\}$ and N(length of the dataset)=12

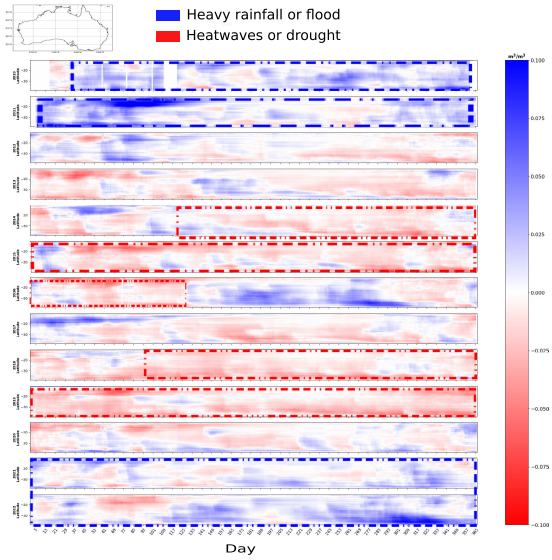

FIGURE 4. Hovmoller plot of SMOS RZSM anomaly for Australia region for a period of 2010 to 2022.

The study mainly focused on the Australian continent because of its diverse climates, ranging from tropical in the north to temperate in the south. This region was selected because of its increased vulnerability to extreme climatic conditions, such as droughts and floods. The Hovmoller plot (Figure 4) shows SM anomalies for different periods such as, 2010-2011 and 2021-2022, where the areas shaded in blue indicate high SM values corresponding to flood events linked to La Niña, [52], [53]. Conversely, for 2014 to 2016 and 2018 to 2019, the regions shaded in red (indicating drought) were aligned with the effects of El Niño [54]. This indicates that the wetting and drying trends of RZSM capture extreme climatic conditions and retain the integrated impact of climatic conditions over an extended period [55].

B. EVALUATION OF SMOS RZSM WITH IN-SITU SM

Figure 5 provides a time series graph from 2011 to 2017 for individual sites for Wankamma (Amma Catch) (a), 1.09 (HOBE) (b), Little River (SCAN) (c), and Mouthoumet (SMOSMANIA)(d). At Wankamma site, SMOS RZSM presents similar seasonal variation to in-situ SM, but SMOS RZSM never reaches the minimum values with in-situ SM, as shown in Figure 5(a) because of the sandier soil texture [56], [57], [58], [59]. In the Little River, the SMOS RZSM exhibited higher SM values than the in-situ SM, as shown in Figure 5(c). This disparity might arise from water percolation at a deeper level, which is affected by the intensity and duration of water events, including watershed characteristics, not captured by the depth of the in-situ SM measurements [45]. In contrast, HOBE (5) and Mouthoumet (Figure 5(d)) showed an increase in SM peak during the growing season of each year, which may be due to irrigation [40]. This is because, on average, these regions receive substantial rainfall, and the monitoring stations do not exhibit a significant response to these precipitation events.

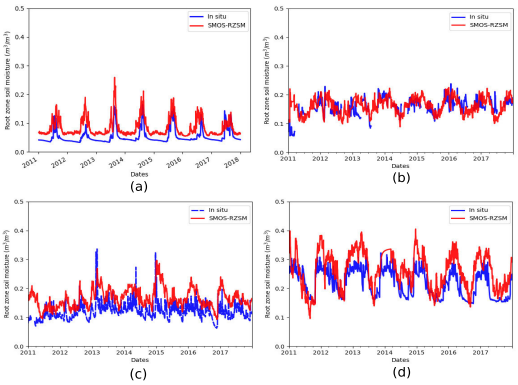

FIGURE 5. Time series graph of in-situ (weighted average) and SMOS RZSM for individual site of Amma Catch (Wankamma site) (a), HOBE (1.09) (b), SCAN (Little river) (c) and SMOSMANIA (Mouthoumet) (d) from 2011 to 2017.

TABLE 2. Statistical results in terms of pearson correlation coefficient (R), mean bias (MB), root mean square difference (RMSD) and unbiased root mean square difference (ubRMSD) for the network Amma Catch, HOBE, SCAN and SMOSMANIA for the period of 2011 to 2017.

Network	Site name	Correlation coefficient (-)	Mean bias (m^3/m^3)	Root mean square difference (m^3/m^3)	Unbiased root mean square difference (m^3/m^3)
Amma Catch	Belefoungou mid	0.93	0.08	0.09	0.04
	Belefoungou top	0.93	0.18	0.09	0.04
	Wankama	0.81	-0.03	0.03	0.02
HOBE	1.03	0.26	-0.01	0.03	0.03
	1.04	0.56	-0.06	0.07	0.03
	1.07	0.53	0.02	0.08	0.08
	1.09	0.41	-0.01	0.03	0.03
	2.01	0.68	-0.05	0.05	0.02
	2.04	0.14	0.05	0.08	0.07
	2.05	0.44	-0.01	0.04	0.04
	2.07	0.52	-0.02	0.04	0.04
	3.01	0.67	0.06	0.07	0.04
	3.02	0.68	0.11	0.13	0.06
	3.04	0.65	0.02	0.06	0.08
	3.07	0.71	0.02	0.09	0.06
SCAN	AllenFarms	0.68	0.13	0.14	0.04
	Ames	0.43	0.24	0.24	0.05
	EastviewFarm	0.58	0.03	0.05	0.04
	LittleRiver	0.58	0.05	0.05	0.03
	PeeDee	0.71	-0.09	0.10	0.03
	PowellGardens	0.67	0.22	0.23	0.06
	SandyRidge	0.53	0.04	0.08	0.06
	ShagarkHills	0.44	0.07	0.11	0.09
	UAPBDewitt	0.61	0.07	0.10	0.06
SMOSMANIA	Lahas	0.82	0.10	0.10	0.06
	Lezignac	0.83	-0.02	0.03	0.02
	Mazan Abbaye	0.75	0.08	0.10	0.07
	Mejannes	0.80	0.01	0.05	0.05
	Montaut	0.68	0.06	0.08	0.05
	Mouthoumet	0.78	-0.05	0.06	0.04
	Narbonne	0.67	0.02	0.06	0.06
	Peyrassegrande	0.84	0.12	0.13	0.03
	Prades Iez	0.68	0.06	0.07	0.04
	Sainfelixde	0.85	0.07	0.08	0.04
	Savenes	0.84	0.06	0.06	0.03
	Urpins	0.84	0.10	0.11	0.04
	Villeville	0.87	0.05	0.08	0.06

Table 2 presents the statistical results between SMOS RZSM and in-situ SM for Pearson correlation coefficient (R), mean bias (MB), root mean square difference (RMSD) and unbiased root mean square difference (ubRMSD). The statistical results are presented for the Amma Catch, HOBE, SCAN, and SMOSMANIA networks from 2010 to 2017. Note that statistical analysis was performed only in terms of temporal variability, as stated in Section III-A. The temporal correlation coefficient between SMOS RZSM and in-situ SM shows in the range (0.83-0.93) for Amma Catch, (0.14 to 0.71) for HOBE, (0.43 to 0.71) for SCAN, and (0.67 to 0.87) for SMOSMANIA. Fisher's z- transform computes the average correlation coefficient for each network [60]. The average correlation coefficients for Amma Catch, HOBE, SCAN and SMOSMANIA are 0.92, 0.54, 0.56 and 0.80, respectively. The analysis shows better performance for the Amma Catch, HOBE, and SMOSMANIA network than for the SCAN network, which indicates the limitation in representing wetlands or grasslands of the selected in-situ sites [61]. The average unbiased root mean square difference (ubRMSD) for all networks was almost 0.04 m^3/m^3, which satisfies the requirements of various applications.

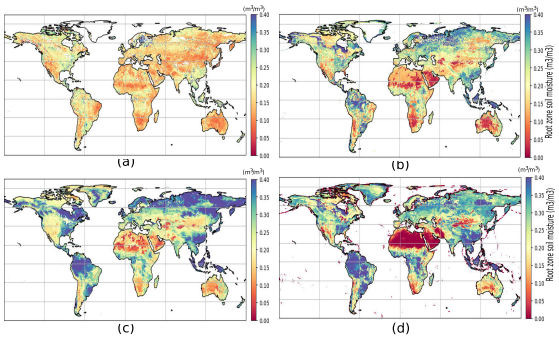

FIGURE 6. Global average root zone soil moisture maps of SMOS-RZSM (a), SMAP-RZSM (b), GLDAS-RZSM (c) and ERA5-RZSM (d) for 2017.

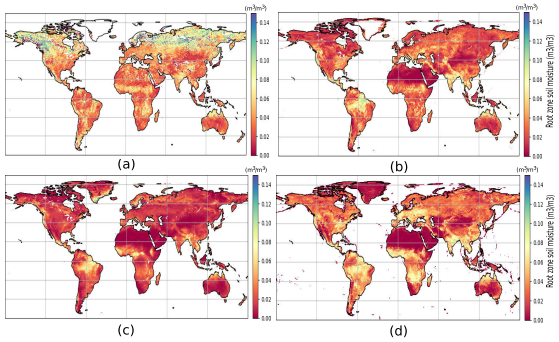

FIGURE 7. Global temporal standard deviation of root zone soil moisture maps of SMOS-RZSM (a), SMAP-RZSM (b), GLDAS-RZSM (c) and ERA5-RZSM (d) for the period of 2017.

C. COMPARISON OF SMOS RZSM PRODUCT WITH ERA5, GLDAS, AND SMAP RZSM PRODUCT

Figure 6 illustrates the temporal average of the global RZSM map for SMOS, SMAP, ERA5, and GLDAS for 2017. The range of SM varied from one RZSM to an other. The range of the RZSM value for the 5 and 95 percentage quantile ranges represents the value of SMOS in the range of 0.09 to 0.29 m^3/m^3, SMAP ranges from 0.04 to 0.41 m^3/m^3, GLDAS ranges from 0.1 to 0.44 m^3/m^3 and ERA5 ranges from 0.0014 to 0.36 m^3/m^3. Comparatively, SMOS shows lower RZSM values, attributed to its reliance on less surface SM during the estimation process [62]. Distinct variations were observed in the polar regions, where SMOS displayed lower RZSM values, and moderate SMAP values, and ERA5 and GLDAS exhibited higher RZSM values. Conversely, ERA5, GLDAS, SMOS, and SMAP RZSM showed a wet bias in tropical forests. The wet bias in ERA5 and GLDAS could arise from modeling inaccuracies or meteorological input variables, particularly precipitation, and sensing constraints in SMOS and SMAP, which influence RZSM retrieval. Figure 7 shows the temporal variability of SMOS, SMAP, GLDAS, and ERA5 RZSM for 2017. Notably, the dry regions exhibited less temporal variation than the wet regions (as seen in Figure 6). For the 75 percent quantile, all RZSM products showed a variability of less than 0.38, except for the SMOS RZSM variability of 0.57. Higher variability in the SMOS RZSM was observed in regions with challenging retrievals such as forests and frozen or snowy areas.

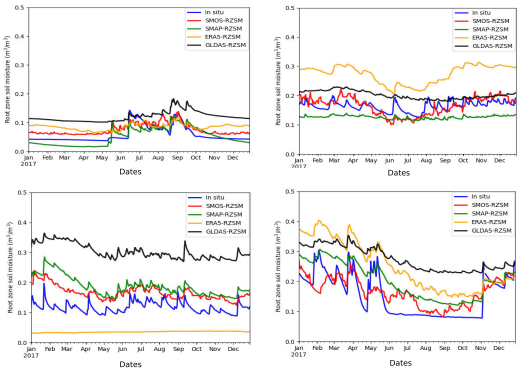

FIGURE 8. Time-series graph of in-situ SM (dotted blue), SMOS (red), SMAP (green), ERA5 (yellow) and GLDAS (black) RZSM for the individual network of Amma Catch(Wankamma site) (a), HOBE (1.01) (b), SCAN (Little river)(c) and SMOSMANIA (Mejannes) (d) for 2017.

Figure 8 shows the time series graphs of the RZSM products (SMOS, SMAP, ERA5, and GLDAS) with the in-situ SM. A time series graph is shown for the four individual sites: Wankamma (Amma Catch), 1.01 (HOBE), Little River (SCAN), and Mejannes (SMOSMANIA) for each RZSM in 2017. At the Wankamma site (Figure 8(a)), all RZSM products with in-situ SM exhibited similar temporal dynamics. However, at 1.01 (HOBE) site (Figure 8(c)), ERA5 was overestimated with in-situ SM and showed minimal temporal dynamics in the Little River (Figure 8(d)). This inaccuracy is due to the inaccurate calibration of the precipitation data due to the distance between the meteorological station and the in-situ site. Overall, SMAP and GLDAS RZSM with in situ-SM show similar temporal dynamics. However, the GLDAS RZSM yielded higher SM values across all sites. This demonstrates that the assimilation approach used in the SMAP RZSM reduced the errors resulting from precipitation, and improved the results in locations with precise precipitation data. Nevertheless, SMAP and GLDAS RZSM were unable to capture the variation in SM dynamics during the growing season in the 1.01 site (HOBE). This demonstrates that despite the advantage of data assimilation in SMAP RZSM, the land surface model is unable to account for shifts in SM dynamics that occurs due to irrigation, which contributes to discrepancies. In contrast, the SMOS and in-situ SM data showed better temporal dynamics than the other RZSM products across all monitoring sites.

Table 3 shows the temporal results between the RZSM and in-situ data for the SMOS, SMAP, GLDAS, and ERA5 RZSM over the Amma Catch, HOBE, SCAN, and SMOSMANIA networks separately for 2017. The statistical results are presented as the Pearson correlation coefficient (R), mean bias (MB), root mean square difference (RMSD) and unbiased root mean square difference (ubRMSD). The Amma Catch and SMOSMANIA networks show comparable performance for all RZSM products, with an average correlation coefficient between RZSM and in-situ SM between 0.62 and 0.97. GLDAS exhibited poor performance over the HOBE network, and ERA5 across the SCAN network displayed a correlation coefficient in the range of -0.03 to 0.79 and -0.13 to 0.60, respectively, as shown in Figure 8. However, SMOS and SMAP showed marginally improved results compared with GLDAS and ERA5, with correlation coefficients in the range of 0.42-0.87. The results demonstrate that the successful integration of satellite observations in SMOS and SMAP RZSM captures the seasonal variability more effectively at the temporal scale than model-based approaches (ERA5 and GLDAS).

TABLE 3. Statistical results in terms of pearson correlation coefficient (R), mean bias (MB), root mean square difference (RMSD) and unbiased root mean square difference (ubRMSD) for SMOS-RZSM, SMAP-RZSM, GLDAS-RZSM and ERA5-RZSM product with in-situ measurements for Amma Catch, HOBE, SCAN and SMOSMANIA networks.

Network	Site	Correlation Coefficient (-)				Mean bias (m^3/m^3)				Root mean square difference (m^3/m^3)				Unbiased root mean square difference (m^3/m^3)			
		SMOS	SMAP	GLDAS	ERA5	SMOS	SMAP	GLDAS	ERA5	SMOS	SMAP	GLDAS	ERA5	SMOS	SMAP	GLDAS	ERA5
Amma Catch	Belefoungou mid	0.95	0.92	0.95	0.97	0.08	-0.02	0.02	-0.17	0.09	0.09	0.05	0.17	0.04	0.05	0.02	0.02
	Belefoungou top	0.95	0.87	0.91	0.97	0.08	0.03	-0.02	-0.17	0.09	0.09	0.05	0.17	0.04	0.05	0.05	0.02
	Wankama	0.83	0.74	0.62	0.64	-0.02	0.01	-0.06	-0.03	0.02	0.02	0.07	0.04	0.02	0.02	0.02	0.02
HOBE	1.03	0.42	0.57	0.21	0.59	-0.01	0.03	-0.05	-0.12	0.03	0.05	0.06	0.12	0.03	0.03	0.03	0.03
	1.04	0.76	0.70	0.40	0.86	-0.05	-0.01	-0.09	-0.17	0.05	0.02	0.09	0.17	0.02	0.01	0.01	0.02
	1.07	0.76	0.71	0.55	0.78	0.05	0.09	0.01	-0.06	0.07	0.11	0.06	0.08	0.05	0.06	0.06	0.04
	1.09	0.52	0.74	0.06	0.63	0	0.04	-0.04	-0.11	0.03	0.04	0.04	0.11	0.03	0.10	0.02	0.02
	2.04	0.91	0.69	-0.03	0.92	0.04	0.08	0	-0.04	0.04	0.09	0.04	0.05	0.02	0.04	0.04	0.02
	2.05	0.87	0.81	0.68	0.85	0	0.03	-0.05	-0.08	0.02	0.04	0.05	0.08	0.02	0.03	0.02	0.02
	3.01	0.86	0.78	0.79	0.86	0.05	0.08	0	-0.03	0.06	0.09	0.04	0.03	0.03	0.05	0.04	0.03
	3.02	0.78	0.77	0.79	0.86	0.14	0.18	0.12	0.08	0.15	0.19	0.13	0.07	0.04	0.06	0.05	0.05
SCAN	AllenFarms	0.43	0.19	0.32	-0.10	0.16	0.03	0.01	0.15	0.16	0.06	0.03	0.16	0.03	0.05	0.02	0.06
	Ames	0.63	0.59	0.52	0.23	0.24	0.17	0.18	0.26	0.25	0.17	0.19	0.27	0.05	0.04	0.03	0.06
	EasternFarm	0.42	0.51	0.35	0.34	0.01	-0.03	-0.10	0.10	0.03	0.05	0.10	0.12	0.03	0.04	0.02	0.05
	LittleRiver	0.46	0.46	0.33	-0.13	-0.05	-0.07	-0.19	0.08	0.05	0.07	0.19	0.08	0.02	0.03	0.03	0.02
	PecDec	0.39	0.61	0.52	0.16	-0.07	0.02	-0.16	0.13	0.07	0.03	0.16	0.13	0.02	0.02	0.03	0.03
	PrairieGardens	0.18	0.76	0.52	0	0.23	0.10	0.11	0.32	0.23	0.10	0.11	0.32	0.04	0.03	0.04	0.05
	SandyRidge	0.52	0.51	0.42	0.27	0.08	-0.06	-0.01	0.23	0.09	0.08	0.03	0.23	0.04	0.05	0.03	0.03
	ShapbarkHills	0.65	0.60	0.47	0.01	0.11	0	0.03	0.05	0.12	0.05	0.06	0.10	0.05	0.05	0.05	0.09
	Tuskegee	0.33	0.58	0.03	0.43	-0.26	0.08	-0.25	0.09	0.27	0.09	0.26	0.11	0.02	0.05	0.02	0.06
	UAPBfewatt	0.75	0.91	0.75	0.60	0.09	0.02	0.02	0.30	0.10	0.03	0.04	0.30	0.03	0.03	0.04	0.04
	WalnutGulch	0.67	0.62	0.71	0.11	-0.04	0.01	-0.07	0.04	0.06	0.02	0.07	0.04	0.04	0.02	0.01	0.02
SMOSMANIA	Lahas	0.82	0.70	0.83	0.89	0.08	-0.10	-0.01	-0.01	0.09	0.09	0.06	0.04	0.05	0.05	0.06	0.04
	Lezignac	0.88	0.70	0.85	0.79	-0.02	-0.01	-0.14	-0.13	0.03	0.03	0.14	0.13	0.02	0.03	0.02	0.03
	Maran abbaye	0.72	0.91	0.87	0.88	0.06	-0.04	-0.01	-0.09	0.09	0.06	0.05	0.10	0.06	0.04	0.05	0.04
	Mejannes	0.79	0.88	0.76	0.76	-0.01	-0.05	-0.12	-0.10	0.04	0.06	0.13	0.11	0.04	0.03	0.05	0.05
	Montaut	0.63	0.90	0.89	0.87	0.03	-0.07	-0.05	-0.10	0.08	0.08	0.08	0.11	0.07	0.05	0.06	0.04
	Mouthomet	0.79	0.66	0.86	0.71	-0.05	-0.02	-0.06	-0.07	0.06	0.04	0.07	0.07	0.03	0.03	0.03	0.03
	Peyrusseguade	0.83	0.71	0.75	0.66	0.12	-0.03	-0.02	0.12	0.12	0.05	0.05	0.04	0.03	0.03	0.04	0.04
	Prades lez	0.72	0.69	0.66	0.72	0.09	0	-0.03	0.05	0.10	0.06	0.06	0.07	0.05	0.06	0.05	0.05
	Saintfelixde	0.74	0.90	0.85	0.84	0.07	-0.02	0.02	0.07	0.09	0.09	0.06	0.08	0.05	0.03	0.05	0.04
	Savenes	0.81	0.83	0.88	0.80	0	-0.04	-0.06	-0.02	0.05	0.05	0.07	0.03	0.03	0.03	0.04	0.03

Figure 9 shows several Taylor diagrams of four RZSM products (SMOS, SMAP, GLDAS, and ERA5) over the in-situ SM networks Amma Catch, HOBE, SCAN, and SMOSMANIA. It displays the quantitative analysis of four RZSM products along with in-situ observations in terms of the Pearson correlation coefficient (black line), root mean square difference (green), and standard deviation (black). ERA5 RZSM over SCAN Networks shows a negative correlation in three in-situ networks with RMSD error above 0.06 and standard deviation less than 0.01 as shown in Figure 5 (c). The GLDAS RZSM showed lower RMSD and less spatial variability than other RZSM products across all networks. The SMAP RZSM better captures the spatial variability across all networks except HOBE, as shown in Figure 5(b). However, in contrast to other RZSM products, the SMOS RZSM better captured the spatial variability observed in all networks.

D. APPLICATION OF RZSM TO DETECT IRRIGATION SIGNALS

Figure 10 presents the RZSM averaged for the dry season (December 2016 to March 2017) for SMOS, SMAP, ERA5, and GLDAS products in the Telangana region. Actually, as the season is marked by an absence of rainfall, the SM spatial distribution is mainly affected by the distribution of the inundated rice growing area extent. The latter was derived using Sentinel-2 observations [42], which are driven by surface and ground water availability [35]. ERA5 and SMOS exhibit a higher and more realistic spatial variability than SMAP and GLDAS, with wetter RZSM along the main perennial rivers where rice driven areas are located (areas covered by more than 60% of rice), and lower RZSM in rain-fed crop dominant areas, where rice covered areas remain

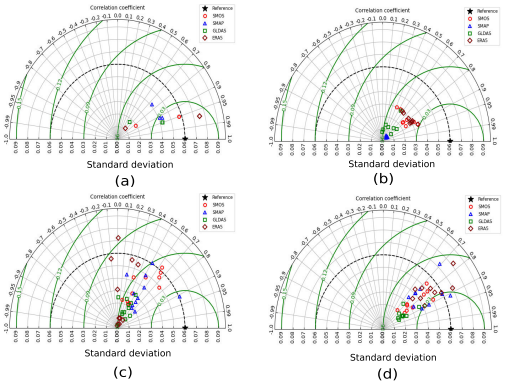

FIGURE 9. The Taylor diagram displays the statistical comparison between RZSM products and in-situ SM over Amma Catch (a), HOBE (b), SCAN (c), and SMOSMANIA (d) in terms of the Pearson correlation coefficient (black line), root mean square difference (green), and standard deviation (black). The RZSM products include the SMOS RZSM (red circles),SMAP RZSM (blue triangles),GLDAS RZSM (green squares), and ERA5 RZSM (brown diamonds).

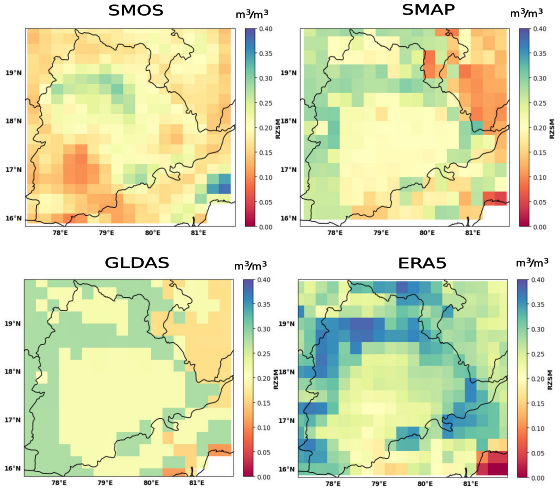

FIGURE 10. Spatial representation of the seasonal RZSM average from December-2016 to March-2017 for SMOS, SMAP, GLDAS and ERA5 RZSM over Telangana region, India.

below 20%. SMOS RZSM is dryer in average compare to ERA5. These results illustrate that assimilation schemes used to retrieve RZSM from irrigated areas should reflect the initial spatial variability of satellite observations used. In other words, as shown by Pascal [45], the SM observation shall correct or drive the model simulation rather than the opposite.

Figure 11 presents the time series of monthly anomalies of the RZSM data (SMOS, SMAP, ERA5, and GLDAS), precipitation, NDVI and percentage of rice cover for irrigated areas from 2016 to 2020. Each RZSM was presented as a monthly anomaly to minimize uncertainties arising from different climatic sources. The rice cover percentage map was computed for the dry season (January-April) [42]. This information helps us to understand the SM dynamics attributed to rice cultivation and its associated water management practices. Monthly NDVI data were used as an indicator of crop or vegetation growth to observe the change in SM due to irrigation. NDVI and SMOS RZSM showed bimodal seasonal patterns associated with changes in wet and dry growth seasons. During the monsoon season, SM increases with precipitation; however, in the dry season, only the SMOS RZSM exhibited an increase in SM peaks. The increase in SM was associated with the increase in NDVI and the rice cover percentage peak, which was attributed to irrigation. A noticeable increase in the percentage of rice cover observed during 2016 and 2018 compared to 2017 was attributed to abundant precipitation during the monsoon season, which led to an increase in the water table level. The increase in the groundwater level provided sufficient water for dry season crops. This shows that model-based (ERA5, GLDAS, and SMAP) RZSM products limit their applicability for detecting irrigation signals with minimal precipitation. This highlights the limitation of the model-based approach, which does not include information regarding un-modeled processes such as irrigation techniques [63]. This also shows the inability of the SMAP RZSM to detect irrigation signals despite using satellite observations for data assimilation. This suggests that the indirect use of SM from temperature brightness in the data-assimilation approach removes the irrigation signal [64], [65].

E. DISCUSSION

This study analyzes the quality of the SMOS RZSM in comparison to in-situ SM and other global RZSM products. This study investigated the benefits of utilizing remote sensing satellite data in conjunction with a simple physical-based approach in estimating RZSM rather than utilizing a more complex model-based approach. In this context, we investigated different RZSM products, including satellite-based (SMOS RZSM), model-based (GLDAS and ERA5 RZSM), and assimilation-based (SMAP RZSM) products.

Wagner et al. [19] first proposed a mathematical equation to estimate an index for the RZSM based on satellite observations, such as ERS scatterometer data, and using a simple bucket model. Ford et al. [20] used this approach to calculate the RZSM from the SMOS surface, demonstrating the usefulness of this approach when the soil characteristics are uniform throughout the soil column. This study used a similar methodology to retrieve the RZSM from SMOS satellite observations on a global scale. The main difference is that this study extended their method to calculate the absolute value of RZSM using a weighted average of RZSM at different depths using soil texture information. SMOS RZSM provides an absolute value of RZSM representing the mean value at depths from 5 to 100 cm worldwide on the EASE 2 grid at a spatial resolution of 25 km on a daily time scale.

This study presents qualitative and quantitative analysis of the SMOS RZSM with in-situ RZSM at a deeper layer to account for the variability of SMOS RZSM over space and time at a global scale. It has been noted that in certain in-situ networks with sandier soil textures, SMOS RZSM exhibits

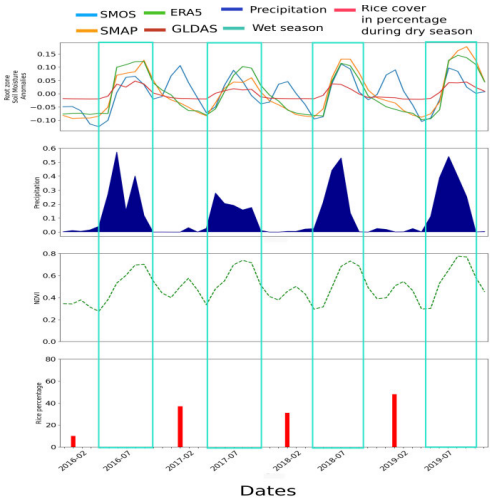

FIGURE 11. Time series of monthly anomalies of SMOS, SMAP, GLDAS and ERA5 RZSM between 2016 to 2019, GPM-IMERG monthly precipitation, MODIS monthly NDVI for the irrigated areas of Telangana region, India. First row: SMOS (blue), SMAP (orange), ERA5 (green), GLDAS (red)in m^3/m^3; second row: precipitation (mm/month); third row: NDVI (green); fourth row: dry season rice percentage.

significant RMSD values. This is because sandier soil is highly permeable and has a low water retention capacity. As a result, water from precipitation seeps into the deeper layer, making the surface layer dryer due to evaporation. This results in high variability in surface SM, which reduces the direct influence of surface SM on the root zone and thus weakens the coupling between the surface SM and the root zone over this region [66].This decoupling is strengthened by various factors including vegetation, climate conditions and soil texture and varies regionally. When the coupling between the surface and RZSM is weaker, SMOS RZSM does not perform well [20].

A comparison of all the RZSM products shows their advantages and disadvantages of each RZSM product. It can be seen that the RZSM approaches based on complex models (GLDAS and ERA5 RZSM) show smaller RMSD values but are less able of accurately capturing spatial variability than the SMAP and SMOS RZSM products. This demonstrates the advantage of using a satellite-based approach (SMOS and SMAP RZSM) over a model-based approach, as satellite remote sensing data better captures spatial variability, which is important for accurate estimation of RZSM on a global scale. The other disadvantage of model-based methods (GLDAS and ERA5 RZSM) is that they lack the ability to detect irrigation signals because the land surface model lacks information on anthropogenic processes such as irrigation. A similar limitation is evident in the SMAP RZSM, as it does not consider un-modeled processes such as irrigation in flood-irrigated areas during the dry season. This weakness of the SMAP RZSM algorithm is attributed to the data assimilation method, which uses the re-scaling method to reduce the large differences between the SM representation in the model and satellite observation [65]. This re-scaling method reduces the systematic differences between the model and the remote sensing satellite observations. Thus, when the increase in SM due to irrigation is observed by the land surface model, it is suppressed by the land surface model, as the model lacks information on un-modeled processes such as irrigation [63]. As a result, the SMAP RZSM model cannot capture the change in SM dynamics that occurs due to irrigation. However, SMOS RZSM has the advantage of capturing changes in SM dynamics that occur due to irrigation because it directly uses surface SM information to estimate RZSM, preserving surface SM information that has been affected by anthropogenic activities such as irrigation. The main limitation of the SMOS RZSM is that it does not accurately estimate the SM in a deeper layer when the coupling between the surface SM and RZSM is weaker. Another drawback of the SMOS RZSM is its dependence on the surface SM, which means that any ambiguity in the surface SM directly affects the RZSM. For example, if the surface SM is extremely dry, the computed RZSM values will likewise be dry, as indicated by the low range of SM values from the SMOS RZSM compared to other products.

In the future, the coupling between the surface and RZSM can be improved by incorporating evapo-transpiration and runoff in the SMOS RZSM estimation, which will continue under different climatic conditions and their effects on different soil moisture depths in the RZSM.

IV. CONCLUSION AND PERSPECTIVE

The SMOS RZSM provides SM data at depths of 5-100 cm globally with a spatial sampling resolution of 25 km on the EASE grid 2. The SMOS RZSM was calculated from the SMOS level-3 surface SM using a simple physical model with the idea of a linear relationship between the surface SM and the root zone. SMOS RZSM data from 2010 to the present are available on the CATDS platform. However, there is a lack of validation of the SMOS RZSM on a global scale and its quality compared to other available model and assimilation-based RZSM products such as ERA5, GLDAS, and SMAP RZSM. In this context, the SMOS RZSM was evaluated using in-situ SM to check the quality of the SMOS RZSM under different climatic conditions. Then, the SMOS RZSM and other RZSM products are evaluated in comparison with in-situ SM to analyze the efficacy of the simple model-based approach (SMOS RZSM) over the model and data-assimilation-based approach (ERA5, GLDAS SMAP) in the retrieval of RZSM. In-situ networks selected from the ISMN were used for this analysis, such as Amma Catch, HOBE, SMOSMANIA, and SCAN networks.

A visual comparison between the SMOS surface SM and SMOS RZSM shows that the SMOS RZSM is less variable in space and time and preserves long-term information. The SMOS RZSM can in turn be used to identify climatic events such as droughts and floods. In the future, this study can be used to detect extreme climatic conditions on a continental or regional scale and to investigate factors that influence the occurrence of extreme events, such as human-induced or climatic factors [67], [68]. Furthermore, the SMOS RZSM

was evaluated using in-situ SM, and the average correlation coefficient between the SMOS RZSM and in-situ SM showed better performance for AMMA CATCH and SMOSMANIA in the range (0.80-0.92). ubRMSD is less than 0.04 m^3/m^3 is observed for clayey soil (loamy, clay loam, clay) and greater than 0.04 m^3/m^3 for sandier soil (loamy sand, sandy loam, sandy clay loam). This shows that the SMOS RZSM algorithm does not perform well over sandier soil because of the weaker coupling between the surface and the RZSM. In the future the estimation of the RZSM algorithm can be improved by including evapo-transpiration and runoff information [69].

A comparison of the complex model, data-assimilation (complex model and satellite observation), or satellite-based RZSM product (ERA5, GLDAS, SMAP, and SMOS RZSM) with in-situ SM shows that the model-based approach (ERA5, GLDAS) does not fully capture the temporal dynamics at the root zone as compared to the simple model- and data- assimilation approach (SMOS and SMAP RZSM). Further comparison in irrigated areas shows that the complex model and data-assimilation-based RZSM products (ERA5, GLDAS, and SMAP RZSM) do not capture the irrigation signal, that is the change in SM dynamics during the dry season, where irrigation depends on water resources. In contrast, a simple model-based approach (SMOS RZSM) with the direct inclusion of SM from satellite observations detects irrigation signals during the dry season. It can be concluded that SMOS RZSM shows a preferable outcome with the explicit use of surface SM observations. In the future, this study will be further investigated at a regional scale for the quantification of irrigation signals by retrieving the RZSM at a kilometer or sub-kilometric scale using high-resolution surface SM.

ACKNOWLEDGMENT

The authors acknowledge the European Space Agency (ESA) for providing the SMOS data. The authors would like to thank Ahmad Al Bitar for this root zone soil moisture algorithm and Stephane Tarot for the implementation at CATDS.

REFERENCES

[1] D. Entekhabi, I. Rodriguez-Iturbe, and F. Castelli, "Mutual interaction of soil moisture state and atmospheric processes," *J. Hydrol.*, vol. 184, nos. 1–2, pp. 3–17, Oct. 1996.

[2] T. J. Jackson, "Profile soil moisture from surface measurements," *J. Irrigation Drainage Division*, vol. 106, no. 2, pp. 81–92, Jun. 1980.

[3] M. Guérif and C. L. Duke, "Adjustment procedures of a crop model to the site specific characteristics of soil and crop using remote sensing data assimilation," *Agricult., Ecosystems Environ.*, vol. 81, no. 1, pp. 57–69, Oct. 2000.

[4] H. Douville, "Relevance of soil moisture for seasonal atmospheric predictions: Is it an initial value problem?" *Climate Dyn.*, vol. 22, no. 4, pp. 429–446, Apr. 2004.

[5] P. A. Dirmeyer, "Using a global soil wetness dataset to improve seasonal climate simulation," *J. Climate*, vol. 13, no. 16, pp. 2900–2922, Aug. 2000.

[6] E. Babaeian, M. Sadeghi, S. B. Jones, C. Montzka, H. Vereecken, and M. Tuller, "Ground, proximal, and satellite remote sensing of soil moisture," *Rev. Geophysics*, vol. 57, no. 2, pp. 530–616, Jun. 2019.

[7] Y. H. Kerr, P. Waldteufel, J.-P. Wigneron, J. Martinuzzi, J. Font, and M. Berger, "Soil moisture retrieval from space: The soil moisture and ocean salinity (SMOS) mission," *IEEE Trans. Geosci. Remote Sens.*, vol. 39, no. 8, pp. 1729–1735, May 2001.

[8] D. Entekhabi et al., "The soil moisture active passive (SMAP) mission," *Proc. IEEE*, vol. 98, no. 5, pp. 704–716, May 2010.

[9] J. Parajka, V. Naeimi, G. Blöschl, W. Wagner, R. Merz, and K. Scipal, "Assimilating scatterometer soil moisture data into conceptual hydrologic models at the regional scale," *Hydrol. Earth Syst. Sci.*, vol. 10, no. 3, pp. 353–368, May 2006.

[10] J. M. Sabater, L. Jarlan, J.-C. Calvet, F. Bouyssel, and P. De Rosnay, "From near-surface to root-zone soil moisture using different assimilation techniques," *J. Hydrometeorology*, vol. 8, no. 2, pp. 194–206, Apr. 2007.

[11] J.-C. Calvet and J. Noilhan, "From near-surface to root-zone soil moisture using year-round data," *J. Hydrometeorology*, vol. 1, no. 5, pp. 393–411, Oct. 2000.

[12] D. Helman, I. M. Lensky, and D. J. Bonfil, "Early prediction of wheat grain yield production from root-zone soil water content at heading using crop RS-met," *Field Crops Res.*, vol. 232, pp. 11–23, Feb. 2019.

[13] K. Gavahi, P. Abbaszadeh, H. Moradkhani, X. Zhan, and C. Hain, "Multivariate assimilation of remotely sensed soil moisture and evapotranspiration for drought monitoring," *J. Hydrometeorology*, vol. 21, no. 10, pp. 2293–2308, Oct. 2020.

[14] S. Manfreda, L. Brocca, T. Moramarco, F. Melone, and J. Sheffield, "A physically based approach for the estimation of root-zone soil moisture from surface measurements," *Hydrol. Earth Syst. Sci.*, vol. 18, no. 3, pp. 1199–1212, Mar. 2014.

[15] S. Ahmad, A. Kalra, and H. Stephen, "Estimating soil moisture using remote sensing data: A machine learning approach," *Adv. Water Resour.*, vol. 33, no. 1, pp. 69–80, Jan. 2010.

[16] R. H. Reichle, R. D. Koster, J. Dong, and A. A. Berg, "Global soil moisture from satellite observations, land surface models, and ground data: Implications for data assimilation," *J. Hydrometeorology*, vol. 5, no. 3, pp. 430–442, Jun. 2004.

[17] Q. Liu, R. H. Reichle, R. Bindlish, M. H. Cosh, W. T. Crow, R. de Jeu, G. J. M. De Lannoy, G. J. Huffman, and T. J. Jackson, "The contributions of precipitation and soil moisture observations to the skill of soil moisture estimates in a land data assimilation system," *J. Hydrometeorology*, vol. 12, no. 5, p. 750, Mar. 2011.

[18] G. Dumedah, J. P. Walker, and O. Merlin, "Root-zone soil moisture estimation from assimilation of downscaled soil moisture and ocean salinity data," *Adv. Water Resour.*, vol. 84, pp. 14–22, Oct. 2015.

[19] W. Wagner, G. Lemoine, and H. Rott, "A method for estimating soil moisture from ERS scatterometer and soil data," *Remote Sens. Environ.*, vol. 70, no. 2, pp. 191–207, Nov. 1999.

[20] T. W. Ford, E. Harris, and S. M. Quiring, "Estimating root zone soil moisture using near-surface observations from SMOS," *Hydrol. Earth Syst. Sci.*, vol. 18, no. 1, pp. 139–154, Jan. 2014.

[21] G. Calamita, L. Brocca, A. Perrone, S. Piscitelli, V. Lapenna, F. Melone, and T. Moramarco, "Electrical resistivity and TDR methods for soil moisture estimation in central Italy test-sites," *J. Hydrol.*, vols. 454–455, pp. 101–112, Aug. 2012.

[22] A. M. Peterson, W. D. Helgason, and A. M. Ireson, "Estimating field-scale root zone soil moisture using the cosmic-ray neutron probe," *Hydrol. Earth Syst. Sci.*, vol. 20, no. 4, pp. 1373–1385, Apr. 2016.

[23] C. Carranza, C. Nolet, M. Pezij, and M. van der Ploeg, "Root zone soil moisture estimation with random forest," *J. Hydrol.*, vol. 593, Feb. 2021, Art. no. 125840.

[24] K. C. Kornelsen and P. Coulibaly, "Root-zone soil moisture estimation using data-driven methods," *Water Resour. Res.*, vol. 50, no. 4, pp. 2946–2962, Apr. 2014.

[25] B. Li et al., "Global GRACE data assimilation for groundwater and drought monitoring: Advances and challenges," *Water Resour. Res.*, vol. 55, no. 9, pp. 7564–7586, Sep. 2019.

[26] H. Hersbach,B. Bell, P. Berrisford, G. Biavati, A. Horányi, J. Muñoz Sabater, J. Nicolas, C. Peubey, R. Radu, I. Rozum, and D. Schepers, "Era5 hourly data on single levels from 1979 to present," *Copernicus climate change service climate data store*, vol. 10, no. 10, p. 24381, 2018.

[27] R. H. Reichle, J. V. Ardizzone, G.-K. Kim, R. A. Lucchesi, E. B. Smith, and B. H. Weiss, "Soil moisture active passive (SMAP) mission level 4 surface and root zone soil moisture (L4_SM) product specification document," Tech. Note, 2022.

[28] A. Ceballos, K. Scipal, W. Wagner, and J. Martínez-Fernández, "Validation of ERS scatterometer-derived soil moisture data in the central part of the duero basin, Spain," *Hydrological Processes*, vol. 19, no. 8, pp. 1549–1566, 2005.

[29] R. Mahmood and K. G. Hubbard, "Relationship between soil moisture of near surface and multiple depths of the root zone under heterogeneous land uses and varying hydroclimatic conditions," *Hydrological Processes*, vol. 21, no. 25, pp. 3449–3462, Dec. 2007.

[30] R. Mahmood, A. Littell, K. G. Hubbard, and J. You, "Observed data-based assessment of relationships among soil moisture at various depths, precipitation, and temperature," *Appl. Geography*, vol. 34, pp. 255–264, May 2012.

[31] P. D. Stroud, *A Recursive Exponential Filter for Time-sensitive Data*, document LAUR-99-5573, 1999.

[32] C. Albergel, C. Rüdiger, T. Pellarin, J.-C. Calvet, N. Fritz, F. Froissard, D. Suquia, A. Petitpa, B. Piguet, and E. Martin, "From near-surface to root-zone soil moisture using an exponential filter: An assessment of the method based on in-situ observations and model simulations," *Hydrol. Earth Syst. Sci.*, vol. 12, no. 6, pp. 1323–1337, Dec. 2008.

[33] A. A. Bitar, A. Mahmoodi, Y. Kerr, N. Rodriguez-Fernandez, M. Parrens, and S. Tarot, "Global assessment of droughts in the last decade from SMOS root zone soil moisture," in *Proc. IEEE Int. Geosci. Remote Sens. Symp. IGARSS*, Jul. 2021, pp. 8628–8631.

[34] M. Pablos, Á. González-Zamora, N. Sánchez, and J. Martínez-Fernández, "Assessment of root zone soil moisture estimations from SMAP, SMOS and MODIS observations," *Remote Sens.*, vol. 10, no. 7, p. 981, Jun. 2018.

[35] C. Pascal, S. Ferrant, N. Rodriguez-Fernandez, Y. Kerr, A. Selles, and O. Merlin, "Indicator of flood-irrigated crops from SMOS and SMAP soil moisture products in Southern India," *IEEE Geosci. Remote Sens. Lett.*, vol. 20, pp. 1–5, 2023, Art. no. 4500205, doi: 10.1109/LGRS.2023.3267825.

[36] J.-C. Calvet, N. Fritz, F. Froissard, D. Suquia, A. Petitpa, and B. Piguet, "In situ soil moisture observations for the CAL/VAL of SMOS: The SMOSMANIA network," in *Proc. IEEE Int. Geosci. Remote Sens. Symp.*, Jun. 2007, pp. 1196–1199.

[37] S. Bircher, N. Skou, K. H. Jensen, J. P. Walker, and L. Rasmussen, "A soil moisture and temperature network for SMOS validation in western Denmark," *Hydrol. Earth Syst. Sci.*, vol. 16, no. 5, pp. 1445–1463, May 2012.

[38] Y. H. Kerr, A. Al-Yaari, N. Rodriguez-Fernandez, M. Parrens, B. Molero, D. Leroux, S. Bircher, A. Mahmoodi, A. Mialon, P. Richaume, S. Delwart, A. Al Bitar, T. Pellarin, R. Bindlish, T. J. Jackson, C. Rüdiger, P. Waldteufel, S. Mecklenburg, and J.-P. Wigneron, "Overview of SMOS performance in terms of global soil moisture monitoring after six years in operation," *Remote Sens. Environ.*, vol. 180, pp. 40–63, Jul. 2016.

[39] T. Lebel, B. Cappelaere, S. Galle, N. Hanan, L. Kergoat, S. Levis, B. Vieux, L. Descroix, M. Gosset, E. Mougin, C. Peugeot, and L. Seguis, "AMMA-CATCH studies in the sahelian region of West-Africa: An overview," *J. Hydrol.*, vol. 375, nos. 1–2, pp. 3–13, Aug. 2009.

[40] S. Bircher, J. E. Balling, N. Skou, and Y. H. Kerr, "Validation of SMOS brightness temperatures during the HOBE airborne campaign, western Denmark," *IEEE Trans. Geosci. Remote Sens.*, vol. 50, no. 5, pp. 1468–1482, May 2012.

[41] G. L. Schaefer, M. H. Cosh, and T. J. Jackson, "The USDA natural resources conservation service soil climate analysis network (SCAN)," *J. Atmos. Ocean. Technol.*, vol. 24, no. 12, pp. 2073–2077, Dec. 2007.

[42] S. Ferrant, A. Selles, M. Le Page, P.-A. Herrault, C. Pelletier, A. Al-Bitar, S. Mermoz, S. Gascoin, A. Bouvet, M. Saqalli, B. Dewandel, Y. Caballero, S. Ahmed, J.-C. Maréchal, and Y. Kerr, "Detection of irrigated crops from Sentinel-1 and Sentinel-2 data to estimate seasonal groundwater use in South India," *Remote Sens.*, vol. 9, no. 11, p. 1119, Nov. 2017.

[43] Y. H. Kerr, P. Waldteufel, P. Richaume, J. P. Wigneron, P. Ferrazzoli, A. Mahmoodi, A. Al Bitar, F. Cabot, C. Gruhier, S. E. Juglea, D. Leroux, A. Mialon, and S. Delwart, "The SMOS soil moisture retrieval algorithm," *IEEE Trans. Geosci. Remote Sens.*, vol. 50, no. 5, pp. 1384–1403, May 2012.

[44] M. J. Brodzik, B. Billingsley, T. Haran, B. Raup, and M. H. Savoie, "EASE-grid 2.0: Incremental but significant improvements for Earth-gridded data sets," *ISPRS Int. J. Geo-Inf.*, vol. 1, no. 1, pp. 32–45, Mar. 2012.

[45] A. Al Bitar, A. Mialon, Y. H. Kerr, F. Cabot, P. Richaume, E. Jacquette, A. Quesney, A. Mahmoodi, S. Tarot, M. Parrens, A. Al-Yaari, T. Pellarin, N. Rodriguez-Fernandez, and J.-P. Wigneron, "The global SMOS level 3 daily soil moisture and brightness temperature maps," *Earth Syst. Sci. Data*, vol. 9, no. 1, pp. 293–315, Jun. 2017.

[46] M. Rodell, P. R. Houser, U. E. A. Jambor, J. Gottschalck, K. Mitchell, C. J. Meng, K. Arsenault, B. Cosgrove, J. Radakovich, M. Bosilovich, and J. K. Entin, "The global land data assimilation system," *Bull. Amer. Meteorological Soc.*, vol. 85, no. 3, pp. 381–394, 2004.

[47] R. Reichle, R. Koster, G. De Lannoy, W. Crow, and J. Kimball, "Level 4 surface and root zone soil moisture (L4_SM) data product," Tech. Note., 2014.

[48] B. J. Cosby, G. M. Hornberger, R. B. Clapp, and T. R. Ginn, "A statistical exploration of the relationships of soil moisture characteristics to the physical properties of soils," *Water Resour. Res.*, vol. 20, no. 6, pp. 682–690, Jun. 1984.

[49] J. Noilhan and J.-F. Mahfouf, "The ISBA land surface parameterisation scheme," *Global Planet. Change*, vol. 13, nos. 1–4, pp. 145–159, Jun. 1996.

[50] M. Piles, J. Ballabrera-Poy, and J. Muñoz-Sabater, "Dominant features of global surface soil moisture variability observed by the SMOS satellite," *Remote Sens.*, vol. 11, no. 1, p. 95, Jan. 2019.

[51] Á. González-Zamora, N. Sánchez, J. Martínez-Fernández, and W. Wagner, "Root-zone plant available water estimation using the SMOS-derived soil water index," *Adv. Water Resour.*, vol. 96, pp. 339–353, Oct. 2016.

[52] P. J. Ward, M. Kummu, and U. Lall, "Flood frequencies and durations and their response to el Niño Southern oscillation: Global analysis," *J. Hydrol.*, vol. 539, pp. 358–378, Aug. 2016.

[53] F. P. D. Delage and S. B. Power, "The impact of global warming and the El Niño-southern oscillation on seasonal precipitation extremes in Australia," *Climate Dyn.*, vol. 54, nos. 9–10, pp. 4367–4377, May 2020.

[54] B. Chapman and K. Rosemond, "Seasonal climate summary for the southern hemisphere (autumn 2018): A weak La Niña fades, the austral autumn remains warmer and drier," *J. Southern Hemisphere Earth Syst. Sci.*, vol. 70, no. 1, pp. 328–352, Nov. 2020.

[55] V. Lakshmi, T. Piechota, U. Narayan, and C. Tang, "Soil moisture as an indicator of weather extremes," *Geophys. Res. Lett.*, vol. 31, no. 11, pp. 1–18, Jun. 2004.

[56] S. Massuel, G. Favreau, M. Descloitres, Y. Le Troquer, Y. Albouy, and B. Cappelaere, "Deep infiltration through a sandy alluvial fan in semiarid Niger inferred from electrical conductivity survey, vadose zone chemistry and hydrological modelling," *CATENA*, vol. 67, no. 2, pp. 105–118, Oct. 2006.

[57] L. Descroix, J.-P. Laurent, M. Vauclin, O. Amogu, S. Boubkraoui, B. Ibrahim, S. Galle, B. Cappelaere, S. Bousquet, I. Mamadou, E. Le Breton, T. Lebel, G. Quantin, D. Ramier, and N. Boulain, "Experimental evidence of deep infiltration under sandy flats and gullies in the Sahel," *J. Hydrol.*, vols. 424–425, pp. 1–15, Mar. 2012.

[58] J. Pfeffer, C. Champollion, G. Favreau, B. Cappelaere, J. Hinderer, M. Boucher, Y. Nazoumou, M. Oï, M. Mouyen, C. Henri, N. Le Moigne, S. Deroussi, J. Demarty, N. Boulain, N. Benarrosh, and O. Robert, "Evaluating surface and subsurface water storage variations at small time and space scales from relative gravity measurements in semiarid Niger," *Water Resour. Res.*, vol. 49, no. 6, pp. 3276–3291, Jun. 2013.

[59] M. Ibrahim, G. Favreau, B. R. Scanlon, J. L. Seidel, M. Le Coz, J. Demarty, and B. Cappelaere, "Long-term increase in diffuse groundwater recharge following expansion of rainfed cultivation in the Sahel, West Africa," *Hydrogeology J.*, vol. 22, no. 6, pp. 1293–1305, Sep. 2014.

[60] R. A. Alexander, "A note on averaging correlations," *Bull. Psychonomic Soc.*, vol. 28, no. 4, pp. 335–336, Oct. 1990.

[61] A. Al Bitar, D. Leroux, Y. H. Kerr, O. Merlin, P. Richaume, A. Sahoo, and E. F. Wood, "Evaluation of SMOS soil moisture products over continental U.S. using the SCAN/SNOTEL network," *IEEE Trans. Geosci. Remote Sens.*, vol. 50, no. 5, pp. 1572–1586, May 2012.

[62] A. Colliander et al., "Performance of SMOS soil moisture products over core validation sites," *IEEE Geosci. Remote Sens. Lett.*, vol. 20, pp. 1–5, 2023.

[63] S. V. Kumar, C. D. Peters-Lidard, J. A. Santanello, R. H. Reichle, C. S. Draper, R. D. Koster, G. Nearing, and M. F. Jasinski, "Evaluating the utility of satellite soil moisture retrievals over irrigated areas and the ability of land data assimilation methods to correct for unmodeled processes," *Hydrol. Earth Syst. Sci.*, vol. 19, no. 11, pp. 4463–4478, Nov. 2015.

[64] P. M. Lawston, J. A. Santanello, and S. V. Kumar, "Irrigation signals detected from SMAP soil moisture retrievals," *Geophys. Res. Lett.*, vol. 44, no. 23, pp. 11–860, Dec. 2017.

[65] Y. Kwon, S. V. Kumar, M. Navari, D. M. Mocko, E. M. Kemp, J. W. Wegiel, J. V. Geiger, and R. Bindlish, "Irrigation characterization improved by the direct use of SMAP soil moisture anomalies within a data assimilation system," *Environ. Res. Lett.*, vol. 17, no. 8, 2022, Art. no. 084006.
[66] S. V. Kumar, R. H. Reichle, R. D. Koster, W. T. Crow, and C. D. Peters-Lidard, "Role of subsurface physics in the assimilation of surface soil moisture observations," *J. Hydrometeorology*, vol. 10, no. 6, pp. 1534–1547, Dec. 2009.
[67] J. F. B. Mitchell, J. Lowe, R. A. Wood, and M. Vellinga, "Extreme events due to human-induced climate change," *Phil. Trans. Roy. Soc. A, Math., Phys. Eng. Sci.*, vol. 364, no. 1845, pp. 2117–2133, Aug. 2006.
[68] K. E. Trenberth, J. T. Fasullo, and T. G. Shepherd, "Attribution of climate extreme events," *Nature Climate Change*, vol. 5, no. 8, pp. 725–730, Aug. 2015.
[69] R. D. Koster, M. J. Suarez, A. Ducharne, M. Stieglitz, and P. Kumar, "A catchment-based approach to modeling land surface processes in a general circulation model: 1. Model structure," *J. Geophys. Res., Atmos.*, vol. 105, no. D20, pp. 24809–24822, Oct. 2000.

NITU OJHA received the M.Sc. degree in geo-informatics and remote sensing from the University of Pune and the Indian Institute of Remote Sensing, Indian Space Research Organisation (ISRO), India, in 2015, and the Ph.D. degree in continental surfaces and interfaces, hydrology, from the Centre d'Etudes Spatiales de la Biosphère (CESBIO), University of Toulouse III-Paul Sabatier, France, in 2021. Her thesis proposed a new technique to provide high-resolution soil moisture products by combining multi-sensor datasets, such as passive microwave, optical/thermal, and active microwave data, at a global scale. She was a Research Assistant with the Geospatial Information Science and Engineering (GISE) Advanced Research Laboratory, Indian Institute of Technology Bombay, India, in 2016. In 2017, she joined as a Research Engineer with the Centre d'Etudes Spatiales de la Biosphère (CESBIO). She joined the SMOS team as a part of the Centre Aval de Traitement des Données SMOS ground segment (CATDS) in CESBIO, in 2021. She is also a part of the Level-4 SMOS Team. Her research interest includes passive microwave remote sensing of continental surfaces.

ALI MAHMOODI received the B.Sc., M.Sc., and Ph.D. degrees in computer science from the University of Toronto, Toronto, ON, Canada, in 1989, 1989, and 1996, respectively. From 1996 to 2014, he was with Array Systems Computing Inc. (Array), Toronto, ON, Canada, as a Project Scientist/Manager. From 2014 to 2021, he was with the Centre d'Etudes Spatiales de la Biosphère (CESBIO), Toulouse, France, as a Research Engineer/Scientist, where he worked mainly on the European Space Agency's (ESA) Soil Moisture and Ocean Salinity (SMOS) mission. At CESBIO, he worked on several projects, including the estimation of root zone soil moisture from SMOS observations. At Array, he has been leading the development and evolution of the SMOS Level 2 Soil Moisture Processor, since 2004. Since 2001, he has been an Adjunct Professor with York University, Toronto, Canada. His teaching portfolio includes introductory courses in programming languages as well as courses in the theory of computation, algorithm analysis, and software design.

ARNAUD MIALON received the Ph.D. degree in ocean-atmosphere-hydrology from Joseph Fourier University, Grenoble, France, and the Ph.D. degree in remote sensing from Université de Sherbrooke, Sherbrooke, QC, Canada, in 2005. In 2006, he joined the Centre d'Etudes Spatiales de la Biosphère, Toulouse, France. He is a part of the soil moisture and ocean salinity (SMOS) satellite mission and especially in soil moisture and VOD retrieval. He is involved with the Centre Aval de Traitement des Données SMOS (CATDS) ground segment. His research interests include passive microwave remote sensing of continental surfaces and their applications in the water cycle.

PHILIPPE RICHAUME received the Engineering degree in computer, electronic, and automatic from École Supérieure d'Informatique, Électronique, Automatique, Paris, France, in 1990, the M.Sc. degree in computer sciences and artificial intelligence from Paul Sabatier University, Toulouse, France, in 1991, and the Ph.D. degree in computer sciences and applied mathematics from CNAM, Paris, in 1996. For the last 25 years, he has worked in various geophysical laboratories, putting to stress advanced computer science and applied mathematics paradigms against real problems, particularly in the remote sensing context. He is currently with the Centre d'Etudes Spatiales de la BIOsphére (CESBIO), Toulouse, France. His research interests include signal processing, nonlinear modeling, and inverse problems, particularly using artificial neural networks, such as for real-time signal processing controller of a radio receiver dedicated to solar wind plasma line tracking onboard the WIND/WAVES spacecraft, or for direct-inverse modeling of ocean surface wind from ERS 1/2 scatterometer or biophysical parameters, LAI, and chlorophyll, from POLDER optical directional reflectance, or using traditional iterative minimization approaches like for soil moisture retrieval from SMOS brightness temperatures he is working on currently, since 2005.

SYLVAIN FERRANT received the Ph.D. degree in agronomy from Univeristé of Toulouse, France, in 2009. He is currently with the Centre d'Etudes Spatiales de la BIOsphére (CESBIO), Toulouse, France. He is working on water availability for agricultural regions by including various agro-hydrological models and long-time series remote sensing data. His research interests include agronomy, hydrology, and carbon cycle in permafrost peat-lands arctic ecosystems.

YANN H. KERR (Life Fellow, IEEE) received the Engineering degree from École Nationale Supérieure de l'Aéronautique et de l'Espace, the M.Sc. degree in electronics and electrical engineering from Glasgow University, Glasgow, Scotland, U.K., and the Ph.D. degree in astrophysique géophysique et techniques spatiales from Université Paul Sabatier, Toulouse, France. From 1980 to 1985, he was with the Centre National d'Etudes Spatiales, Paris, France. In 1985, he joined Laboratoire d'Etudes et de Recherches en Télédétection Spatiale (LERTS), where he was the Director, in 1993 and 1994. He spent 19 months with the Jet Propulsion Laboratory, Pasadena, CA, USA, in 1987 and 1988. Since 1995, he has been with the Centre d'Etudes Spatiales de la Biosphère (CESBIO), Toulouse, where he has been the Deputy Director (1995–1999) and the Director (2007–2016). He was an EOS Principal Investigator (interdisciplinary investigations) and Principal Investigator and precursor of the use of the SCAT over land. In 1989, he started working on the interferometric concept applied to passive microwave earth observation and was subsequently the Science Lead on the MIRAS project for ESA with MMS and OMP. He was also a Co-Investigator on IRIS, OSIRIS, and HYDROS for NASA. He was a Science Advisor for MIMR and Co-Investigator on AMSR. In 1997, he first proposed the natural outcome of the previous MIRAS work with what was to become the SMOS Mission to CNES, a proposal which was selected by ESA, in 1999, with him as the SMOS mission Lead Investigator and the Chair of the Science Advisory Group. He is also the in-charge of the SMOS science activities coordination in France. He is involved with many space missions. His research interests include the theory and techniques for microwave and thermal infrared remote sensing of the earth, with emphasis on hydrology, water resources management, and vegetation monitoring. He has organized all the SMOS Science workshops. He is a member of the SMAP Science Team. He has organized the SMOS workshops and was a guest editor on three IEEE Special issues and one RSE. He is currently involved in the exploitation of SMOS data, in the Cal Val activities and related level 2 soil moisture and level 3 and 4 development and SMOS Aquarius SMAP synergistic uses and on the soil moisture and biomass essential climate variable. He is also working on the SMOS-HR concepts and is/was involved in both the Aquarius and SMAP missions. He was nominated Highly Cited Scientist by Thomson Reuters/Publons, in 2015, 2019, 2020, 2021, 2022, and 2023.